Contemporary Mathematics
Volume 157, 1994

ON THE NUMERICAL SOLUTION OF THE HELMHOLTZ EQUATION AT LARGE WAVE NUMBERS USING EXACT CONTROLLABILITY METHODS. APPLICATION TO SCATTERING

M. O. Bristeau[1], R. Glowinski[2] and J. Periaux[3]

Abstract

The main goal of this article is to introduce a novel method for solving the Helmholtz equations from Acoustics and two-dimensional Electro-Magnetics. The key idea of the method is to go back to the original wave equation and look for time periodic solutions. In order to find these last solutions we essentially use a least squares/shooting method which is closely related to exact controllability and to the Hilbert Uniqueness Method (HUM) of J. L. Lions. From this formulation and by analogy with other controllability problems we derive a conjugate gradient algorithm (in an appropriate Hilbert space) which has quite good convergence properties. Numerical experiments concerning the scattering of planar waves by convex or nonconvex obstacles show the efficiency of the new algorithm, particularly for air intake-like reflectors.

1. Introduction

Stealth technologies have enjoyed a considerable growth of interest during these last five years both for aircraft and space applications. From this point of view an interesting phenomenon

---

1991, *Mathematical Subject Classification:* Primary 65K10, 65M60; Secondary 93C20.

A detailed version of this article will be submitted for publication elsewhere.

0271-4132/94 $1.00 + $.25 per page

has been taking place, namely Fluid Dynamics specialists becoming deeply involved in Computational Electro-Magnetics, which makes sense after all since there are many commonalities between these two topics (see, e.g. [1]). Due to the very high frequencies used by modern radars the computation of the *Radar Cross Section* (RSC) of a full aircraft using the Maxwell equations is still a Great Challenge (see [2]). From the fact that *boundary integral methods* are not well suited to general coated materials, *field approaches* seem to provide an alternative which is worth exploring.

In this paper we consider a particular application of the J. L. Lions *Hilbert Uniqueness Method* (HUM) to the solution of the *Helmholtz equations* obtained when looking to the *monochromatic solutions* of *linear wave problems.* The idea here is to go back to the original wave equation and to apply HUM in order to find its time periodic solutions. Indeed, this new method is in competition with — and is related to — the one where one integrates the wave equation from 0 to $+\infty$ in order to obtain asymptotically a time periodic solution; it is well known from Lax-Phillips [3] that if the scattering body is *convex* then the solution will converge at *exponential* speed to the periodic solution. On the other hand, for *nonconvex* reflectors (which is quite a common situation) the convergence can be very slow; the method described in this paper substantially improves the speed of convergence of the asymptotic one, particularly for stiff problems where internal rays can be trapped by successive reflections.

2. The Helmholtz Equation and its Equivalent Wave Problem

Let us consider a scattering body B, of boundary $\partial B=\gamma$, illuminated by an *incident monochromatic wave* of frequency $f=k/2\pi$ (see Fig. 2.1).

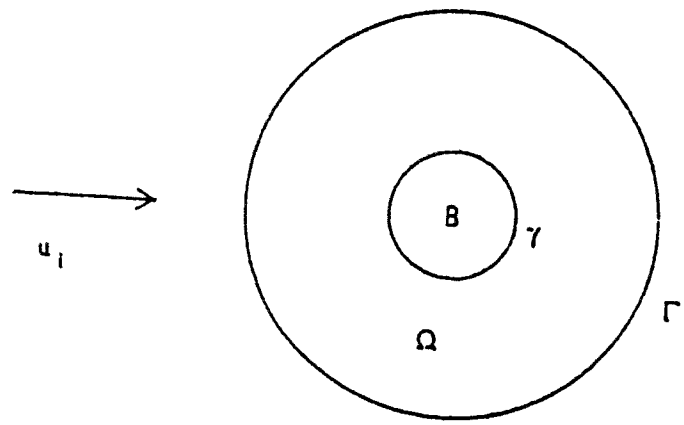

Figure 2.1
(u_i: incident field)

In the case of the wave equation $u_{tt}-\Delta u=0$, the Helmholtz equation satisfied by the coefficient $U(x)$ of e^{ikt} is given by

$$\Delta U + k^2 U = 0 \text{ in } \mathbb{R}^d \backslash \bar{B} \ (d=2,3), \tag{2.1}$$

$$U = G \text{ on } \gamma. \tag{2.2}$$

In practice, we bound $\mathbb{R}^d\backslash\bar{B}$ by an artificial boundary Γ on which we prescribe, for example, an *approximate first order Sommerfeld condition* such that

$$\frac{\partial U}{\partial n} + ikU = 0 \text{ on } \Gamma; \tag{2.3}$$

now equation (2.1) is prescribed on Ω only, where Ω is this portion of $\mathbb{R}^d\backslash\bar{B}$ between γ and Γ. In the above equations, U is the scattered field, $-G$ is the incident field; in general, U and G are *complex valued* functions.

System (2.1)$-$(2.3) is related to the T-periodic solutions ($T=2\pi/k$) of the following wave equation and associated boundary conditions

$$u_{tt} - \Delta u = 0 \text{ in } Q \ (=\Omega\times(0,T)), \tag{2.4}$$

$$u = g \text{ on } \sigma \ (=\gamma\times(0,T)), \tag{2.5}$$

$$\frac{\partial u}{\partial n} + \frac{\partial u}{\partial t} = 0 \text{ on } \Sigma \ (=\Gamma\times(0,T)), \tag{2.6}$$

with, in (2.5), $g(x,t)=g_1(x)\cos kt+g_2(x)\sin kt$, where g_1 and g_2 are two *real valued* functions obtained from the real and imaginary parts G_1 and G_2 of G. If we look for $u=\mathrm{Re}(e^{ikt}U)$ (resp. $u=\mathrm{Im}(e^{ikt}U)$), then it is clear that g satisfies (2.5) with

$$g(x,t) = G_1(x)\cos kt - G_2(x)\sin kt, \text{ (resp. } g(x,t) = G_2(x)\cos kt + G_1(x)\sin kt).$$

The main goal of this article is to find periodic solutions to system (2.4)$-$(2.6) *without* solving the Helmholtz problem (2.1)$-$(2.3).

In the following, we look for T-periodic solutions to systems such as (2.4)$-$(2.6) where g is a *smooth* function of t defined over σ such that $g(0) = g(T)$, $g_t(0) = g_t(T)$, we look thus for u satisfying (2.4)$-$(2.6) and

$$u(0) = u(T),\ u_t(0) = u_t(T). \tag{2.7}$$

In this article we systematically use the notation $\varphi(t)$ for the function $x\longrightarrow\varphi(x,t)$, for any function φ of x and t.

3. Exact Controllability Methods for the Calculation of Time Periodic Solutions to the Wave Equation

In order to solve problem (2.4)−(2.7) we advocate the following approach whose main merit is to reduce the above problem to *an exact controllability* one, close to those problems whose solution is discussed at length in, e.g., [4]−[9]. Indeed, problem (2.4)−(2.7) is clearly equivalent to the following one:

Find $\mathbf{e} = \{e_0, e_1\}$ *such that*

$$u_{tt} - \Delta u = 0 \text{ in } Q, \tag{3.1}$$

$$u = g \text{ on } \sigma, \tag{3.2}$$

$$\frac{\partial u}{\partial n} + \frac{\partial u}{\partial t} = 0 \text{ on } \Sigma, \tag{3.3}$$

$$u(0) = e_0,\ u_t(0) = e_1, \tag{3.4}$$

$$u(T) = e_0,\ u_t(T) = e_1. \tag{3.5}$$

Problem (3.1)−(3.5) is an *exact controllability* problem which can be solved by methods directly inspired by the J. L. Lions *Hilbert Uniqueness Method* (HUM). We shall not address here the existence and uniqueness of solutions to problem (3.1)−(3.5); instead we shall focus on the practical calculations of such solutions, assuming they do exist.

4. Least-Squares Formulation of Problem (3.1)−(3.5)

In order to apply HUM to the solution of problem (3.1)−(3.5) a right choice for the space E containing $\mathbf{e}=\{e_0, e_1\}$ is fundamental. We advocate to take either

$$E = H^1(\Omega) \times L^2(\Omega) \tag{4.1}$$

or

$$E = V_g \times L^2(\Omega), \tag{4.2}$$

where

$$V_g = \{\varphi | \varphi \in H^1(\Omega),\ \varphi|_\gamma = g(0)\}.$$

In order to solve (3.1)−(3.5) we use the following *least squares* formulation (where y plays the role of u in (3.1)−(3.5)):

$$\operatorname*{Min}_{v \in E} J(v), \tag{4.3}$$

with

$$J(v) = \frac{1}{2} \int_\Omega [|\nabla(y(T) - v_0)|^2 + |y_t(T) - v_1|^2]dx,\ \forall v = \{v_0, v_1\}, \tag{4.4}$$

where, in (4.4), the function y is the solution of

$$y_{tt} - \Delta y = 0 \text{ in } Q, \tag{4.5}$$

$$y = g \text{ on } \sigma, \tag{4.6}$$

$$\frac{\partial y}{\partial n} + \frac{\partial y}{\partial t} = \text{on } \Sigma, \tag{4.7}$$

$$y(0) = v_0,\ y_t(0) = v_1. \tag{4.8}$$

The choice of J is directly related to the fact that the natural *energy* $E(\cdot)$ associated to the system is defined by

$$E(t) = \frac{1}{2}\int_\Omega [|y_t|^2 + |\nabla y|^2]dx.$$

Assuming that e is solution of problem (4.3) it will satisfy the following equation

$$<J'(e), v> = 0,\ \forall v \in E_0, \tag{4.9}$$

where $E_0 = E$ if E is defined by (4.1), and where $E_0 = V_0 \times L^2(\Omega)$ (with $V_0 = \{\varphi | \varphi \in H^1(\Omega),\ \varphi|\gamma = 0\}$) if E is defined by (4.2); in (4.9), $<\cdot,\cdot>$ denotes the duality pairing between E_0' and E_0 (E_0': dual space of E_0). In (4.9), J' denotes the *derivative* of J.

Problem (4.9) can be solved by a *conjugate gradient algorithm* (described in Section 6); in order to implement this algorithm, we need to be able to compute $J'(v)$, $\forall v \in E$; this is the object of the following Section 5.

5. Calculation of J'.

It can be shown that

$$\left\{ \begin{aligned} <J'(v), w> = &\int_\Omega \nabla(v_0 - y(T)) \cdot \nabla w_0 dx - \int_\Omega p_t(0) w_0 dx + \int_\Gamma p(0) w_0 d\Gamma \\ &+ \int_\Omega p(0) w_1 dx + \int_\Omega (v_1 - y_t(T)) w_1 dx, \forall w = \{w_0, w_1\} \in E_0, \end{aligned} \right. \tag{5.1}$$

where, in (5.1), p is the solution of the *adjoint equation*

$$p_{tt} - \Delta p = 0 \text{ in } Q, \tag{5.2}$$

$$p = 0 \text{ on } \sigma, \tag{5.3}$$

$$\frac{\partial p}{\partial n} - \frac{\partial p}{\partial t} = 0 \text{ on } \Sigma, \tag{5.4}$$

$$p(T) = y_t(T) - v_1, \tag{5.5}$$

with $p_t(T)$ defined by

$$\int_\Omega p_t(T) z dx = \int_\Gamma (y_t(T) - v_1) z d\Gamma - \int_\Omega \nabla(y(T) - v_o) \cdot \nabla z dx, \ \forall z \in V_o. \tag{5.6}$$

Remark 5.1: Relations (5.1) and (5.6) are largely "formal"; however, it is worth mentioning that the discrete variants of them make sense and lead to algorithms with fast convergence properties.

6. Conjugate Gradient Solution of the Least-Squares Problem (4.3).

In this section we shall suppose that E is defined by (4.2). A *conjugate gradient algorithm* for the solution of (4.9) is given then by

Step 0: Initialization

$$e^o = \{e_o^o, e_1^o\} \in E \text{ is given.} \tag{6.1}$$

Solve the following forward wave problem

$$y_{tt}^o - \Delta y^o = 0 \text{ in } Q, \tag{6.2}_1$$

$$y^o = g \text{ on } \sigma, \tag{6.2}_2$$

$$\frac{\partial y^o}{\partial n} + \frac{\partial y^o}{\partial t} = 0 \text{ on } \Sigma, \tag{6.2}_3$$

$$y^o(0) = e_o^o, \ y_t^o(0) = e_1^o. \tag{6.2}_4$$

Solve the following backward wave problem

$$p_{tt}^o - \Delta p^o = 0 \text{ in } Q, \tag{6.3}_1$$

$$p^o = 0 \text{ on } \sigma, \tag{6.3}_2$$

$$\frac{\partial p^o}{\partial n} - \frac{\partial p^o}{\partial t} = 0 \text{ on } \Sigma, \tag{6.3}_3$$

with $p^o(T)$ *and* $p_t^o(T)$ *given by*

$$p^o(T) = y_t^o(T) - e_1^o, \tag{6.3}_4$$

$$\int_\Omega p_t^o(T) z dx = \int_\Gamma p^o(T) z d\Gamma - \int_\Omega \nabla(y^o(T) - e_o^o) \cdot \nabla z dx, \ \forall z \in V_o, \tag{6.3}_5$$

respectively.

Define next $\mathbf{g}^o = \{g_o^o, g_1^o\} \in E = V_o \times L^2(\Omega)$ *by*

$$(6.4)_1 \qquad \int_\Omega \nabla g_o^o \cdot \nabla z dx = \int_\Omega \nabla(e_o^o - y^o(T)) \cdot \nabla z dx - \int_\Omega p_t^o(0) z dx + \int_\Gamma p^o(0) z d\Gamma, \quad \forall z \in V_o,$$

$$(6.4)_2 \qquad g_1^o = p^o(0) + e_1^o - y_t^o(T),$$

and then

$$(6.5) \qquad \mathbf{w}^o = \mathbf{g}^o. \quad \square$$

For $n \geq 0$ *suppose that* $\mathbf{e}^n$, $\mathbf{g}^n$, $\mathbf{w}^n$ *are known; we compute then their updates* $\mathbf{e}^{n+1}$, $\mathbf{g}^{n+1}$, $\mathbf{w}^{n+1}$ *as follows*

Step 1: Descent

Solve

$$(6.6)_1 \qquad \overline{y}_{tt}^n - \Delta \overline{y}^n = 0 \text{ in } Q,$$

$$(6.6)_2 \qquad \overline{y}^n = 0 \text{ on } \sigma,$$

$$(6.6)_3 \qquad \frac{\partial \overline{y}^n}{\partial n} + \frac{\partial \overline{y}^n}{\partial t} = 0 \text{ on } \Sigma,$$

$$(6.6)_4 \qquad \overline{y}^n(0) = w_o^n, \ \overline{y}_t^n(0) = w_1^n.$$

Solve the following backward wave problem

$$(6.7)_1 \qquad \overline{p}_{tt}^n - \Delta \overline{p}^n = 0 \text{ in } Q,$$

$$(6.7)_2 \qquad \overline{p}^n = 0 \text{ on } \sigma,$$

$$(6.7)_3 \qquad \frac{\partial \overline{p}^n}{\partial n} - \frac{\partial p^o}{\partial t} = 0 \text{ on } \Sigma,$$

with $\overline{p}^n(T)$ *and* $\overline{p}_t^n(T)$ *given by*

$$(6.7)_4 \qquad \overline{p}^n(T) = \overline{y}_t^n(T) - w_1^n,$$

$$(6.7)_5 \qquad \int_\Omega \overline{p}_t^n(T) z dx = \int_\Gamma \overline{p}^n(T) z d\Gamma - \int_\Omega \nabla(\overline{y}^n(T) - w_o^n) \cdot \nabla z dx, \ \forall z \in V_o,$$

respectively.

Define next $\overline{\mathbf{g}}^n = \{\overline{g}_o^n, \overline{g}_1^n\} \in V_o \times L^2(\Omega)$ *by*

$$(6.8)_1 \quad \int_\Omega \nabla \bar{g}_o^n \cdot \nabla z dx = \int_\Omega \nabla(w_o^n - \bar{y}^n(T)) \cdot \nabla z dx - \int_\Omega \bar{p}_t^n(0) z dx + \int_\Gamma \bar{p}^n(0) z d\Gamma, \ \forall z \in V_o,$$

$$(6.8)_2 \quad \bar{g}_1^n = \bar{p}^n(0) + w_1^n - \bar{y}_t^n(T)$$

and then ρ_n *by*

$$(6.9) \quad \rho_n = \int_\Omega [|\nabla g_o^n|^2 + |g_1^n|^2] dx \Big/ \int_\Omega (\nabla \bar{g}_o^n \cdot \nabla w_o^n + \bar{g}_1^n w_1^n) dx.$$

We update then e^n *and* g^n by

$$(6.10) \quad e^{n+1} = e^n - \rho_n w^n,$$

$$(6.11) \quad g^{n+1} = g^n - \rho_n \bar{g}^n.$$

Step 2: Test of the convergence and construction of the new descent direction

If $\int_\Omega (|\nabla g_o^{n+1}|^2 + |g_1^{n+1}|^2) dx / \int_\Omega (|\nabla g_o^o|^2 + |g_1^o|^2) dx \leq \epsilon$ *take* $e = e^{n+1}$; *if not compute*

$$(6.12) \quad \gamma_n = \int_\Omega (|\nabla g_o^{n+1}|^2 + |g_1^{n+1}|^2) dx \Big/ \int_\Omega (|\nabla g_o^n|^2 + |g_1^n|^2) dx$$

and update w^n *by*

$$(6.13) \quad w^{n+1} = g^{n+1} + \gamma_n w^n. \quad \square$$

Do $n = n+1$ *and go to* (6.6).

Remark 6.1: Algorithm (6.1)–(6.13) looks complicated at first glance. In fact, it is not that complicated to implement since each iteration requires basically the solution of two wave equations such as (6.6) and (6.7) and of an elliptic problem such as $(6.8)_1$. The above problems are classical ones for which efficient solution methods already exist.

Remark 6.2: Algorithm (6.1)–(6.13) can be seen as a variation of the method mentioned in Section 1; there, we integrate the periodically excited wave equation until we reach a periodic solution. What algorithm (6.1)–(6.13) does is to *periodically* measure the *lack (or defect) of periodicity* and use this measure as a *residual* to speed up the convergence to a periodic solution. A similar idea was used in [10] to compute the periodic solutions of systems of *stiff* nonlinear differential equations (including cases where the period itself was an unknown of the problem).

7. A Finite Difference/Finite Element Implementation

The practical implementation of the above control based method is straightforward. It is based on a *time discretization* by a *centered second order* in time *explicit finite difference* scheme. This scheme is combined to *piecewise linear finite element* approximations for the space variables; we use *mass lumping* — through numerical integration by the *trapezoidal rule* — to obtain a *diagonal* mass matrix for the acceleration terms. The fully discrete scheme has to satisfy a *stability condition* such as $\Delta t \leq Ch$, where C is a constant. To obtain accurate solutions we need to have h at least *ten times smaller* than the wavelength; consequently, Δt has to be at least ten times smaller than the period. If we assume that the number of iterations to solve the least squares problem is independent of h and Δt (assumption supported by numerical experiments), the solution of the Helmholtz equation via the new approach involves a number of operations which — for a given value of k — is proportional to the number of grid points; for this estimate we do not take into account the time spent at solving the elliptic problems such as $(6.4)_1$, $(6.8)_1$.

8. Numerical experiments.

In order to validate the methods discussed in the above sections we have considered the solution of three test problems of increasing difficulty, namely the scattering of planar incident waves by a disk, a similar problem for a two dimensional ogive and finally the scattering of a planar wave by a *nonconvex* reflector which can be seen as a semi-open cavity (a kind of — very — idealized air intake).

First Test Problem: For this problem, B is a disk of radius .25 m, $k=2\pi f$ with $f=2.4\times10^9$Hz implying that the wavelength λ is .125 m; the disk is illuminated by an incident planar wave coming from the right. The artificial boundary Γ is located at a 3λ distance from B, as shown in Figure 8.1, where we have also shown the finite element triangulation $\mathcal{T}_h$ used for the calculation. This triangulation has 22,736 triangles and 11,588 vertices. The mean length of the edges is $\lambda/14$, the minimal value is $\lambda/38$, while the maximal one is $\lambda/7$ (which is really at the limit of fineness if one wishes a good precision). The value of Δt corresponds to 35 time steps per period. To obtain convergence of the iterative method, 71 iterations of algorithm (6.1)–(6.13) were needed, corresponding to 3mm15s on CRAY2. For this test problem where the exact solution is known we have compared on Figures 8.2 to 8.4 the computed solution (—) to the exact one (....) (we have shown the real component of the scattered fields measured in three different space directions (incident direction, opposite to incident direction, orthogonal direction, respectively)). The convergence behavior has been visualized on Figures 8.5 (decay of the cost function) and 8.6 (variation of the gradient of the cost function).

Second Test Problem: For this problem, B has an ogive-like shape defined by axis parameters a=.6m and b=.16m, respectively. We also have $k=2\pi f$ with f=3GHz implying that the wavelength λ is .1m. The artificial boundary is located at a 3λ distance from B, as shown on Figure 8.7. The finite element triangulation has 14,224 triangles and 7,323 vertices, and is also shown on Figure 8.7. The mean length of the edges if $\lambda/11$, the minimal length is $\lambda/29$, while the maximal one is $\lambda/6$ (which is the limit for an acceptable accuracy). The value of Δt corresponds to 30 times steps per period. The convergence of the solution algorithm for a zero-degree incident monochromatic wave requires 89 iterations corresponding to 2mm13s on a CRAY2. The computed scattered fields are shown on Figures 8.8 (real component) and 8.9 (imaginary component); the space periodicity of the solution is clear on these figures. As expected, the asymptotic unsteady method provides the same solution which, for this *convex* body, is reached exponentially.

Third Test Problem: For this problem, B is an *idealized air intake*; it has a semi-open cavity geometry defined by two horizontal plates (length 4λ and thickness $\lambda/5$) and a vertical one (length 1.4λ and thickness $\lambda/5$). We have $k=2\pi f$ with f=1.2 Ghz, implying that the wave length is .25 m. The artificial boundary is located — again — at a 3λ distance from B, as shown on Fig. 8.10. The finite element triangulation has 33,237 triangles and 16,975 vertices, and is also shown on Figure 8.10. The mean length of the edges in the external region is $\lambda/12.5$, while it is $\lambda/16$ inside the cavity to obtain acceptable accuracy. The value of Δt corresponds to 50 time steps per period. The convergence to the solution for illuminating monochromatic waves of incidence $\alpha=0^o$ and 30^o is shown on Figures 8.11 and 8.12, respectively. We observe that the first solution ($\alpha=0^o$) requires only 100 iterations while the second one ($\alpha=30^o$), with multiple internal reflections, needs 200 iterations of algorithm (6.1)−(6.13); we have also visualized the convergence of the asymptotic method. The contour lines of the computed scattered and total fields (actually, their imaginary component) are shown on Figures 8.13 and 8.14, respectively, for $\alpha=30^o$; the space periodicity is clear on these figures. For this stiff case and in particular at high angle of illumination of the scatter by radar waves (30 degrees and more) the control based method seems definitely more robust and efficient than the asymptotic one as shown on Figures 8.15(a) and (b); this type of behavior has been observed for different complicated geometries including non convexity or curvature effects, while the two methods give very similar computed time periodic solutions for simpler geometries like the one in Figures 8.16 (control method) and 8.17 (asymptotic method) in the case of an open cavity. An interesting phenomenon appears during the convergence process for large values of the incidence; indeed, the convergence curve shows a tendency to flatten, due to the fact that some residual modes with large amplitude are hard to damp before reaching again a "nice" convergence behavior.

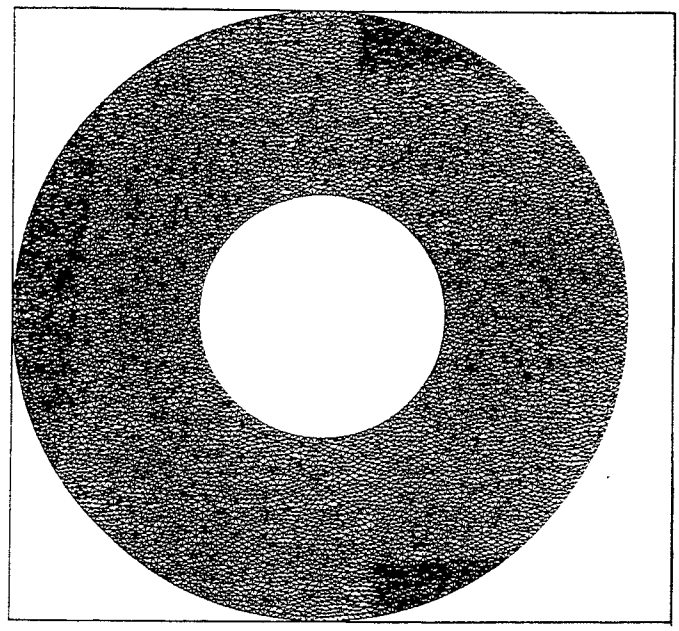

Figure 8.1: First Test Problem:
The computational domain and its triangulation
(11,588 vertices, 22,736 triangles)

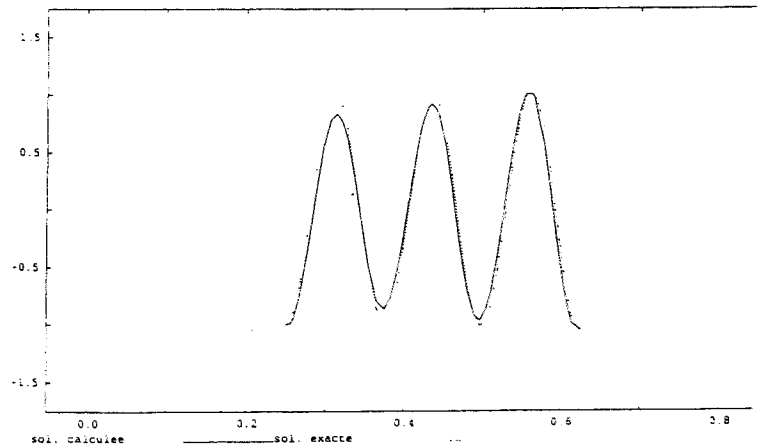

Figure 8.2: First Test Problem:
Variation of the Scattered Field
(incident direction)

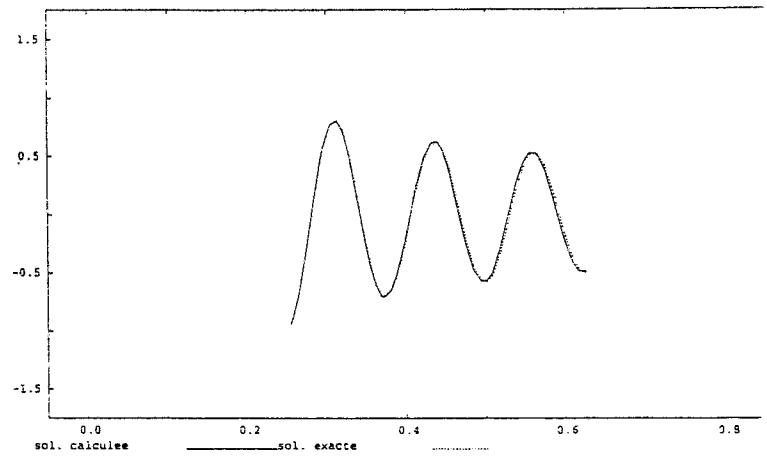

Figure 8.3: First Test Problem:
Variation of the Scattered Field
(opposite to incident direction)

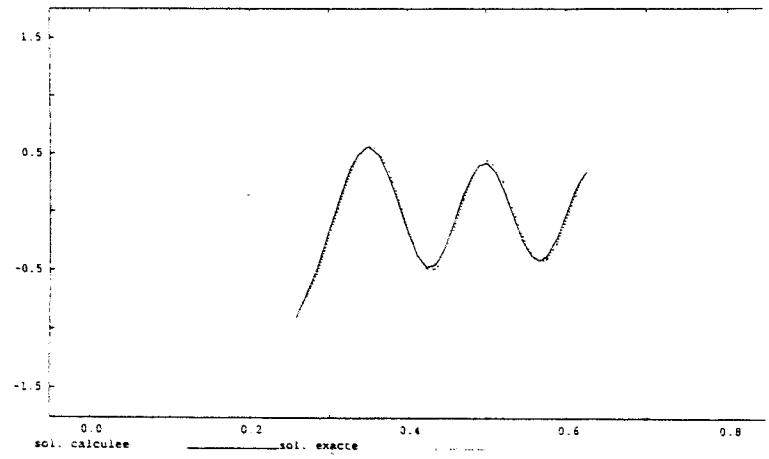

Figure 8.4: First Test Problem:
Variation of the Scattered Field
(orthogonal direction)

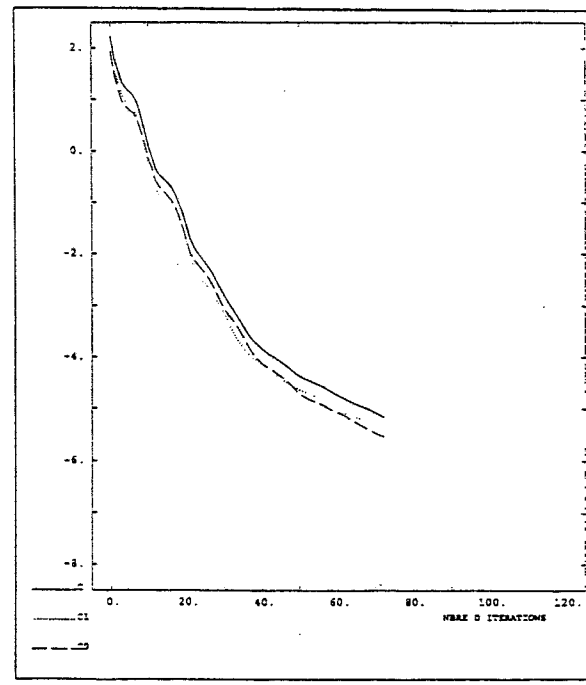

Figure 8.5: First Test Problem:
Variation of the cost function

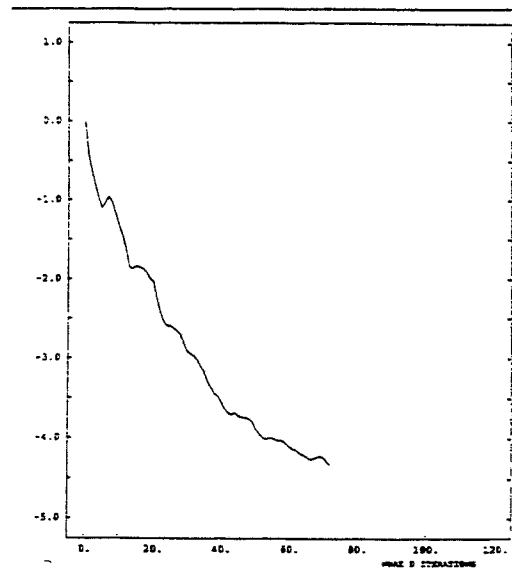

Figure 8.6: First Test Problem:
Variation of the normalized gradient of the cost function

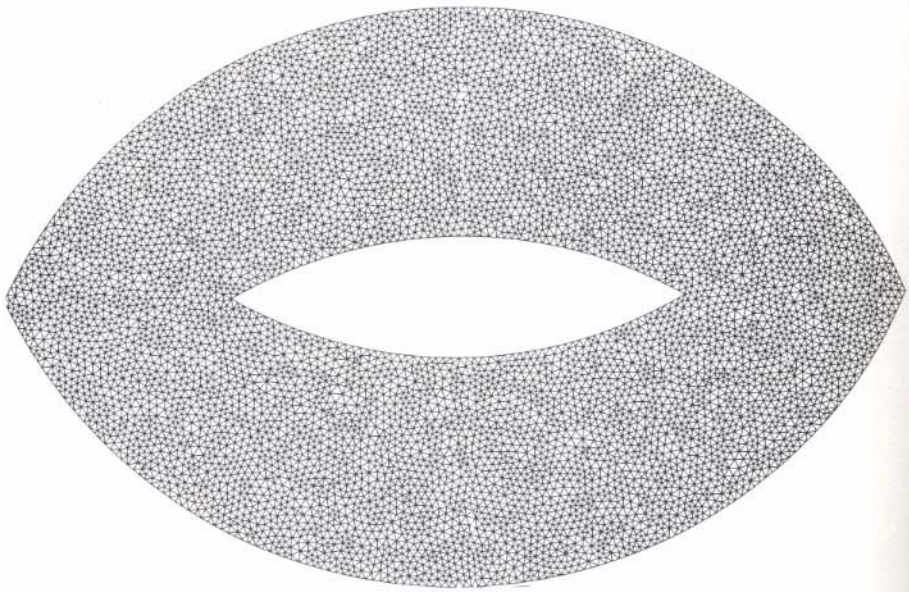

Figure 8.7: Second Test Problem:
Computational Domain and its Triangulation
(7,323 vertices, 14,224 triangles)

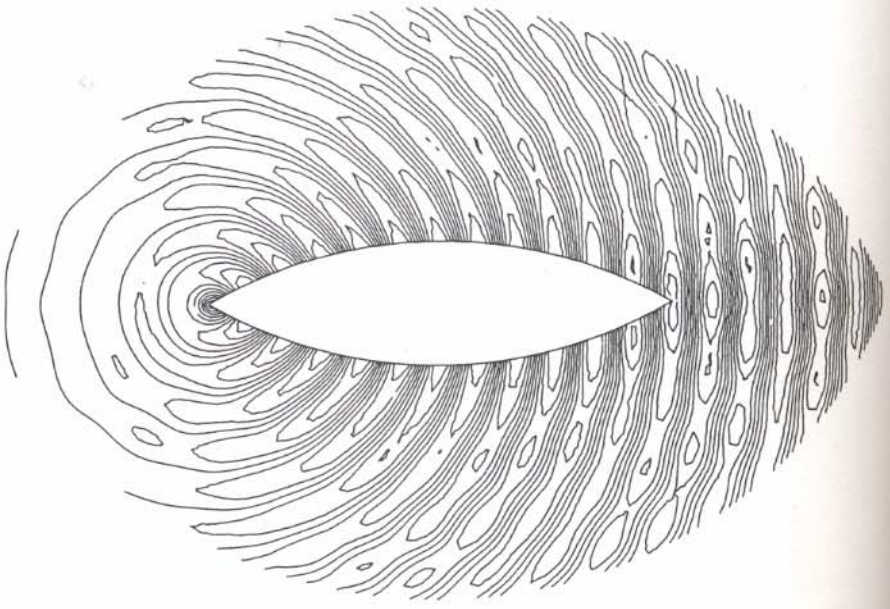

Figure 8.8: Second Test Problem:
Contours of the Scattered Field
(real component)

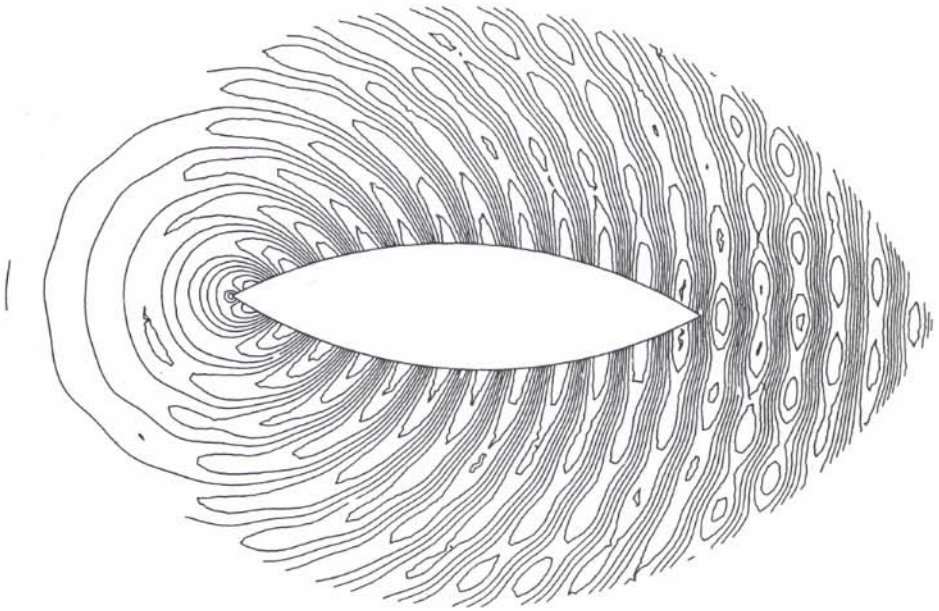

Figure 8.9: Second Test Problem:
Contours of the Scattered Field
(imaginary component)

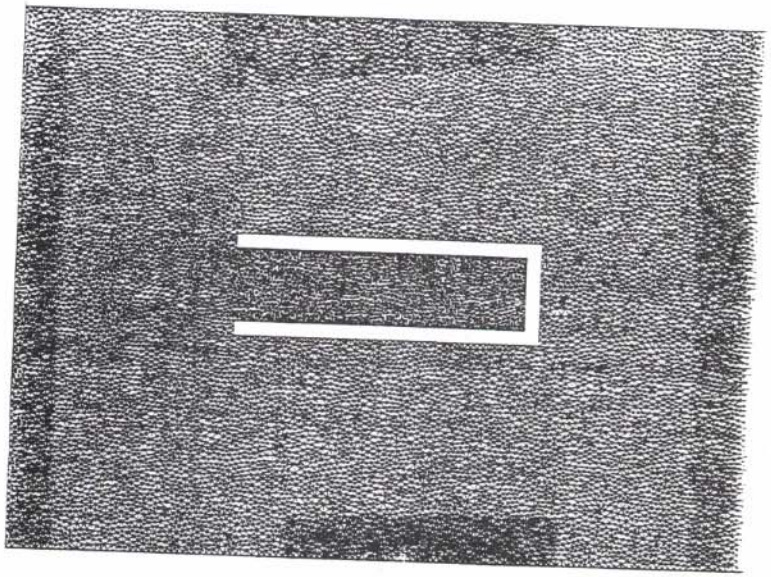

Figure 8.10: Third Test Problem:
The computational problem and its triangulation
(16,975 vertices, 33,237 triangles)

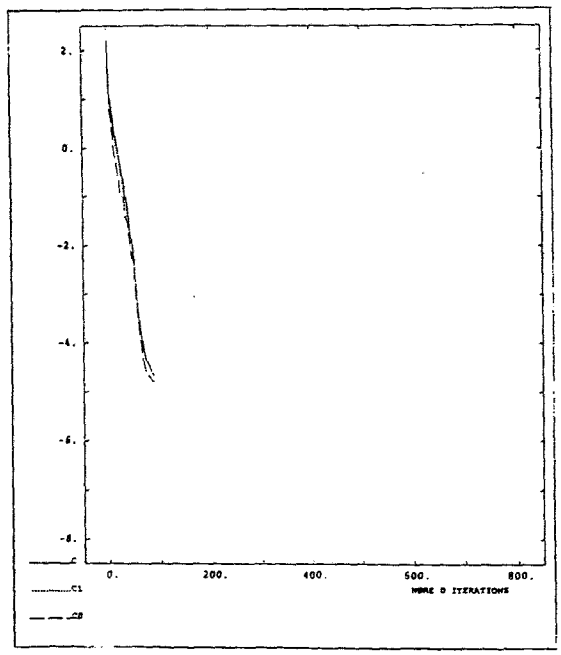

Figure 8.11: Third Test Problem:
Variation of the cost function ($\alpha=0^o$)

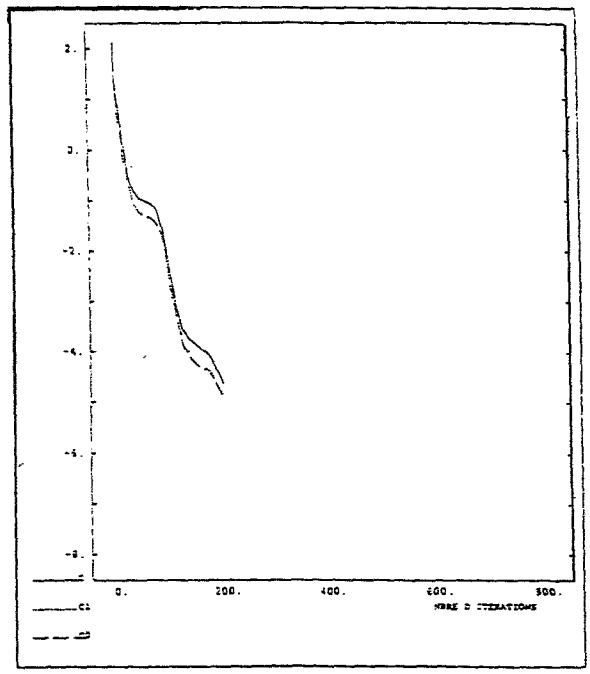

Figure 8.12: Third Test Problem:
Variation of the cost function ($\alpha=30^o$)

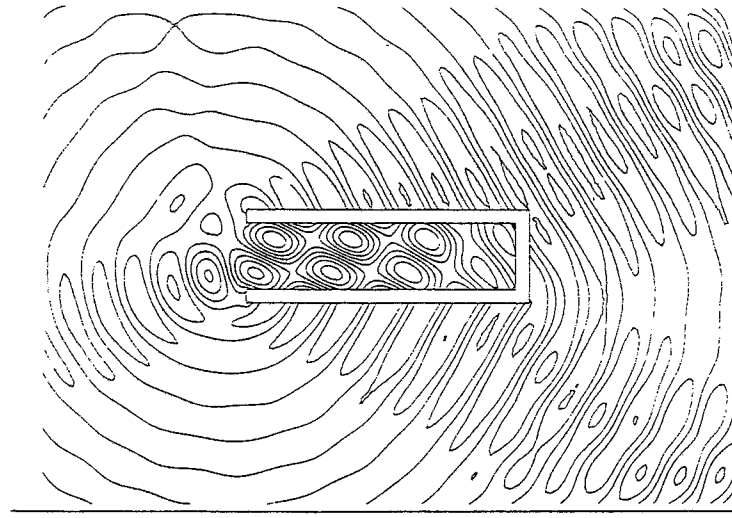

Figure 8.13: Third Test Problem ($\alpha=30^{o}$):
Contours of the scattered field
(imaginary component)

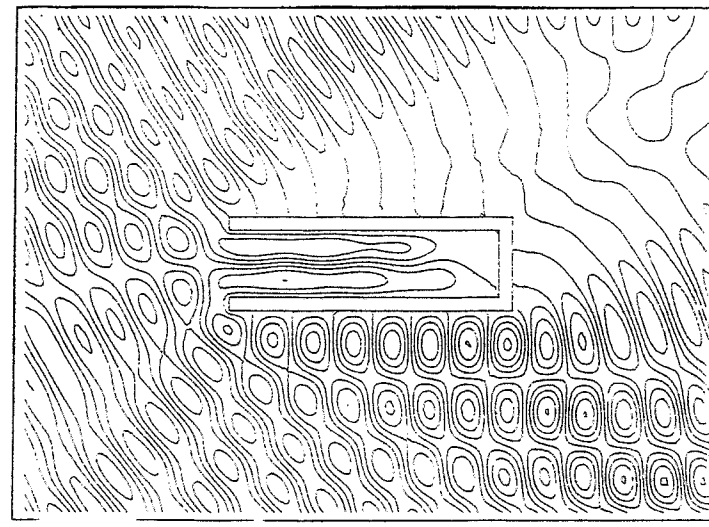

Figure 8.14: Third Test Problem ($\alpha=30^{o}$):
Contours of the total field
(imaginary component)

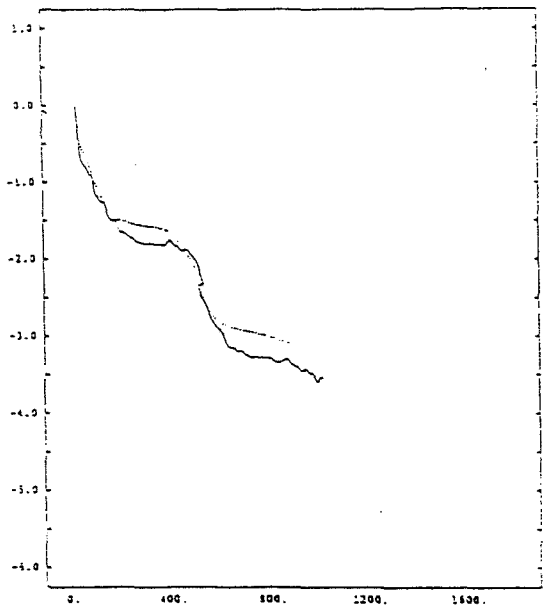

Figure 8.15 (a): Third Test Problem ($\alpha=30^{o}$)
Variation of the Periodicity Residuals (Control Solution)
(−): Displacement residual; (....): Velocity residual

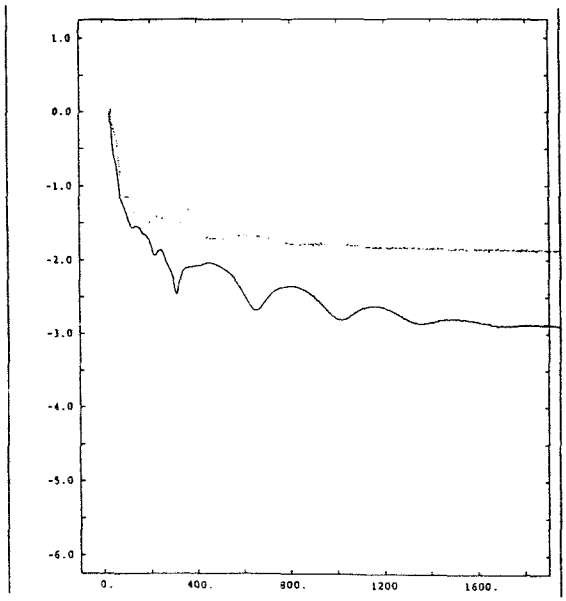

Figure 8.15 (b): Third Test Problem ($\alpha=30^{o}$)
Variation of the Periodicity Residuals (Asymptotic Solution)
(−): Displacement residual; (....): Velocity residual

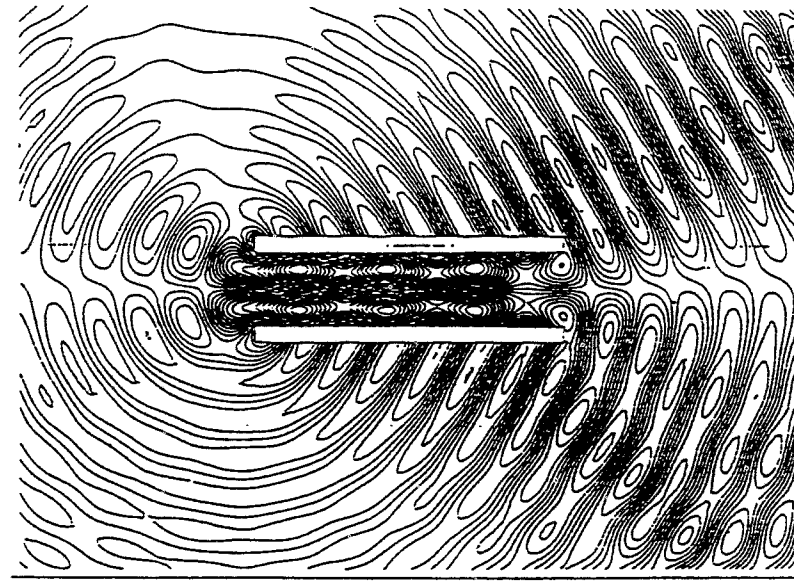

Figure 8.16: Open Cavity Problem
Contours of the Scattered Field
(real component, Control Method)

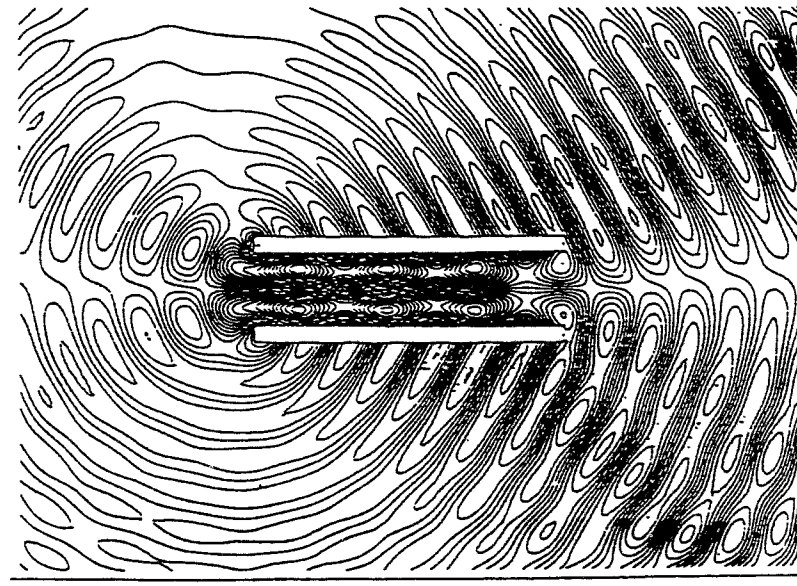

Figure 8.17: Open Cavity Problem
Contours of the Scattered Field
(real component, Asymptotic Method)

9. Further Comments and Conclusion.

We have discussed in this paper a *control* based novel method to solve Helmholtz and two-dimensional harmonic Maxwell equations for *large wave numbers* and for complicated geometries. The new method appears to be more efficient than the traditional computational methods which are based on either time asymptotic behavior, or Linear Algebra algorithms for very large indefinite linear systems.

This new methodology looks promising for three dimensional Maxwell equations and for heterogeneous media. For very large problems, it is likely that we shall have to combine it to *domain decomposition* and/or *fictitious domain* methods, and also to higher order approximations to reduce the number of grid points.

Acknowledgment: The authors would like to thank Professor J. L. Lions and Dr. J. Erhel for helpful comments and suggestions. The support of INRIA, University of Houston, Dassault Aviation, DRET, NSF (Grant INT8612680), DARPA (Contract AFOSR 900334) and Texas Board of Higher Education (Grant 003652156 ARP) is also acknowledged. Finally, special thanks are due to J. A. Wilson for processing this article.

References

[1] D. P. YOUNG, R. G. MELVIN, M. B. BIETERMAN, F. T. JOHNSON, S. S. SAMANTH, J. E. BUSSOLETTI, A locally refined finite rectangular grid finite element method. Application to Computational Physics, *J. Comp. Physics*, 92 (1991), pp. 1-66.

[2] A. TAFLOVE, Reinventing electromagnetics. Supercomputing solution of Maxwell equations via direct time integration and space grid, 30th AIAA Aerospace Sciences Meeting, Reno, Nevada, paper 92-0333.

[3] P. D. LAX & R. S. PHILLIPS, *Scattering Theory*, Academic Press, 1989

[4] J. L. LIONS, Exact Controllability, stabilization and perturbations for distributed systems, *SIAM Review*, 30 (1988), 1-68.

[5] J. L. LIONS, *Controlabilitè Exacte, Perturbations et Stabilisation des Systèmes Distribuès*, Volumes 1 and 2, Masson, Paris, 1988.

[6] R. GLOWINSKI, C. H. LI, J. L. LIONS, A numerical approach to the exact boundary controllability of the wave equation (I) Dirichlet controls: Description of the numerical methods, *Japan J. Appl. Math.*, 7, (1990), pp. 1-76.

[7] R. GLOWINSKI, C. H. LI, On the Exact Neumann Boundary Control of Wave Equations, in *Mathematical and Numerical Aspects of Wave Propagation Phenomena*, G. Cohen, L. Halpern, P. Joly eds., SIAM, Philadelphia, 1991, pp. 15-24.

[8] R. GLOWINSKI, C. H. LI, On the numerical implementation of the Hilbert Uniqueness Method for the exact boundary controllability of the wave equation, *C. R. Acad. Sc.*, Paris, T. 311, Serie I, 1990, pp. 135-142.

[9] E. DEAN, R. GLOWINSKI, C. H. LI, Supercomputer solutions of partial differential equation problems in Computational Fluid Dynamics and in Control, *Computer Physics Communications*, 53, (1989), pp. 401-439.

[10] G. AUCHMUTY, E. DEAN, R. GLOWINSKI, S. C. ZHANG, Control Methods for the Numerical Computation of Periodic Solutions of Autonomous Differential Equations, in *Control Problems for Systems Described by Partial Differential Equations and Applications*, I. Lasiecka, R. Triggiani eds., Lecture Notes in Control and Information Sciences, Vol. 97, Springer-Verlag, Berlin, 1987, pp. 64—89.

---

(1) I.N.R.I.A., Domaine de Voluceau, B.P. 105, 78153 Le Chesnay Cedex, France

(2) Department of Mathematics, University of Houston, Houston, Texas 77204-3476; University of Paris VI, Paris, France, and CERFACS, Toulouse, France

(3) Dassault Aviation, 78, Quai Marcel Dassault, 92214 Saint-Cloud, France.